


Article

Solution Combustion Synthesis of Fe₂O₃-Based Catalyst for Ammonia Synthesis

Binxiang Cai, Huazhang Liu and Wenfeng Han * 

Institute of Industrial Catalysis, Zhejiang University of Technology, Hangzhou 310014, China; cbxloveqjh@163.com (B.C.); cuihua@zjut.edu.cn (H.L.)

* Correspondence: hanwf@zjut.edu.cn; Tel.: +86-571-8832-0063

Received: 23 June 2020; Accepted: 2 September 2020; Published: 7 September 2020



Abstract: Fe₂O₃-based catalysts were prepared by solution combustion synthesis (SCS) with metal nitrates (Fe, K, Al, Ca) as the precursors and glycine as the fuel. The activities of catalysts were evaluated in terms of ammonia synthesis reaction rate in a fixed bed reactor similar to the industrial reactors. The results indicate that the precursor of catalyst prepared by SCS is Fe₂O₃ which facilitates the high dispersion of promoters to provide high activity. The catalysts exhibit higher activity for ammonia synthesis than that of traditional catalysts, and the reaction rate reaches 138.5 mmol g⁻¹ h⁻¹. Fe₂O₃ prepared by SCS could be favorable precursor for ammonia synthesis catalyst. The present study provides a pathway to prepare catalyst for ammonia synthesis.

Keywords: ammonia synthesis; catalyst; Fe₂O₃; solution combustion synthesis

1. Introduction

The development of a commercial catalytic process for ammonia synthesis was one of the most significant technological breakthroughs of the 20th century [1]. However, ammonia synthesis via Haber-Bosch process is an energy intensive industry as it requires high operating temperatures (400–500 °C) and high pressures (15–30 MPa) over iron (Fe₃O₄ or Fe_{1-x}O) catalysts [1]. Energy saving and emission reduction is the eternal theme of the ammonia synthesis industry, and its core technology is the ammonia synthesis catalyst. Therefore, it is important to search for new and more efficient catalysts for ammonia synthesis.

The molten iron catalyst uses iron oxide as a precursor, and iron oxides have three forms, namely Fe₂O₃, Fe₃O₄, and FeO. The traditional iron catalysts with Fe₃O₄ as precursor have been widely studied for more than 100 years. By the end of the 1970s, this catalyst was considered to be well consolidated and no special improvement was still expected, forcing people to look for new technological breakthroughs of the jumping type [2].

A new type of wustite-based catalysts (WBC) was discovered by Liu et al. in 1986 [3,4]. WBC is the first significant innovation in the industrial iron-based catalyst for ammonia synthesis after the development of catalysts for the Haber-Bosch process in 1910. Much higher activity and a lower reaction temperature than the traditional magnetite-based catalysts (MBC) were achieved [5]. It was shown that the reaction rate of the new catalyst is 70–90% higher than that of the traditional one. So, WBC appears to be competitive with Ru/C. This is a high energy consumption process for preparing iron catalysts by the melting method. The Fe_{1-x}O catalyst has been used commercially for many years, but it seems to have encountered a bottleneck in its research. It is very difficult for the Fe_{1-x}O catalyst to select and optimize the promoters.

Fe₂O₃ will decompose under high temperature melting conditions: 3Fe₂O₃ = 2Fe₃O₄ + 0.5O₂. It cannot be prepared by melting method. Fe₂O₃-based ammonia synthesis catalysts prepared by the precipitation method have been reported in many studies, but their activity is the lower than that of

Fe₃O₄-based catalysts. The preparation of Fe₂O₃-based catalysts by solution combustion synthesis (SCS) has been rarely reported.

Solution combustion synthesis (SCS) was reported as an efficient method for the preparation of nanomaterials [6]. Actually, SCS is allowed for the production of nanosized, homogeneous crystalline powders without the risk of contamination and is environmentally friendly since the byproducts of the synthesis are CO₂, NO₂, and H₂O. In addition, the yield is high (95%) [7]. During SCS, fuel plays a major role in the formation of nanomaterials. Fuel usually forms complexes with the metal ions facilitating the homogeneous mixing of the metal ions in solution. The SCS yields nano-size oxide materials as either volume or layer-by-layer propagating combustion modes depending on the type of the precursors, as well as the conditions used for the process organization [8–10]. We have prepared Cr₂O₃ nanoparticles by SCS which exhibited high performance for dehydrofluorination of 1,1,1,3,3-Pentafluoropropane to 1,3,3,3-Tetrafluoropropane [11].

In the present work, we propose that Fe₂O₃ is also an efficient precursor of the catalyst for ammonia synthesis. In addition, the effect of the glycine/Fe ratio on the structural-microstructural-morphological properties and on the distribution of promoters of the Fe₂O₃ prepared by SCS was investigated. The performance of Fe₂O₃-based catalysts was compared with the WBC catalyst prepared by the melting method.

2. Results and Discussion

2.1. Morphology and Phase Structure of Catalysts

XRD patterns of the catalysts prepared by SCS and the WBC catalyst are displayed in Figure 1 with no other impurities detected, indicating that all the promoters are uniformly dispersed in the parent phase. The phase structure of WBC before reduction was identified as FeO (PDF#06-0615) (Figure 1a). However, the phase structure composition of SCS catalysts varies with the composition of glycine/Fe. The phase of SCS1.7, SCS2.5, and SCS3.3 agree well with γ -Fe₂O₃, and the phases of SCS5 and SCS8.3 are very similar to α -Fe₂O₃. Obviously, following the different composition of glycine/Fe and different preparation routes, different phase structures of iron oxides are obtained. γ -Fe₂O₃ is formed when the fuel (glycine) is insufficient, and α -Fe₂O₃ is formed when the fuel (glycine) is sufficient. There are great differences in the structure of iron oxides with different crystal structures. FeO belongs to cubic NaCl structure, α -Fe₂O₃ belongs to a hexagonal corundum structure and γ -Fe₂O₃ belongs to a cubic spinel structure.

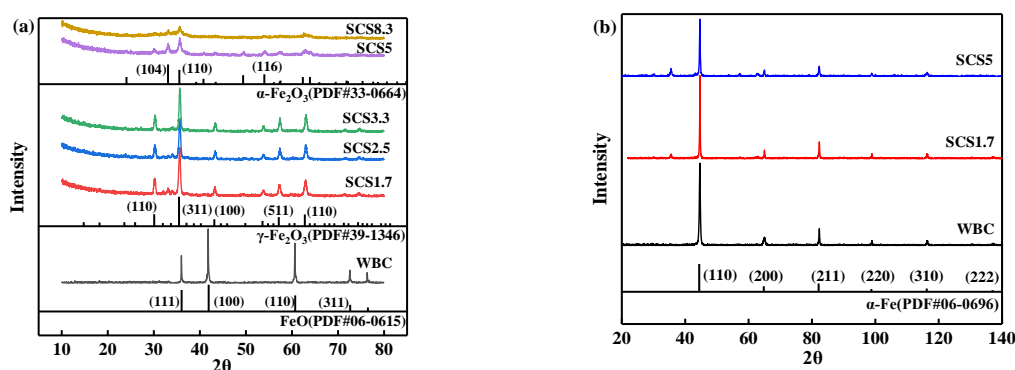


Figure 1. XRD patterns of SCS and WBC catalysts (a) fresh catalysts and (b) reduced catalysts.

The phase of all reduced catalysts is α -Fe, as shown in Figure 1b. For all catalysts, the diffraction peaks of promoters are not detected, indicating the high dispersion of all promoters in the catalyst. Some clear but not indexed diffraction peaks are seen in the SCS1.7 and SCS5 catalysts (at 2 theta ca. 29, ca. 35, ca. 59, and ca. 62). When the reduced catalyst is removed from the reactor, α -Fe is oxidized by oxygen in the atmosphere, these diffraction peaks may belong to iron oxide. Another important

effect observed in Figure 1 is that the intensity of the XRD peaks decreases gradually with glycine/Fe ratio. This might be due to an increase of the microstrain and/or to a decrease of the crystal size.

The crystal size of the catalysts was calculated by Scherer formula as shown in Tables 1 and 2. The crystal size of fresh catalysts is displayed in Table 1. As listed in Table 1, the average crystal size of SCS5 and SCS8.3 catalysts is 16.3 nm and 16.0 nm, respectively. The average crystal size of WBC is around 26.9 nm, which is much larger than the SCS.

Table 1. Crystal size of fresh catalysts.

Catalyst	Crystal Size /nm					
	D _{100(FeO)}	D _{110(FeO)}	D _{110(γ-Fe₂O₃)}	D _{311(γ-Fe₂O₃)}	D _{104(α-Fe₂O₃)}	D _{110(α-Fe₂O₃)}
WBC	28.0	25.7	–	–	–	–
SCS1.7	–	–	13.9	18.4	–	–
SCS5	–	–	–	–	18.6	14.0
SCS8.3	–	–	–	–	16.2	15.8

Table 2. Crystal size of reduced catalysts.

Catalyst	Crystal Size /nm					Ratios	
	D ₁₁₀	D ₂₀₀	D ₂₁₁	D ₂₂₀	D ₃₁₀	D ₂₂₂	D ₂₁₁ / D ₁₁₀
WBC	22.7	15.2	37.2	55.5	45.6	39.5	1.64
SCS1.7	33.7	27.2	28.3	32.0	29.0	40.9	0.84
SCS5	14.6	20.4	19.8	23.1	17.9	14.2	1.36

The ammonia synthesis reaction is a typical structure sensitive reaction. The catalytic activity is closely related to particle size, crystal morphology and crystal plane index. It is well accepted that the order of catalytic activity for ammonia synthesis on the crystal face of α -Fe follows (111) > (211) > (100) > (210) > (110) [12]. Among them, the catalytic activity of the (111) face is 400 times higher than that of (110) face. However, the (111) crystal plane cannot be detected by XRD. Consequently, a (211) crystal plane is adopted to correlate the performance.

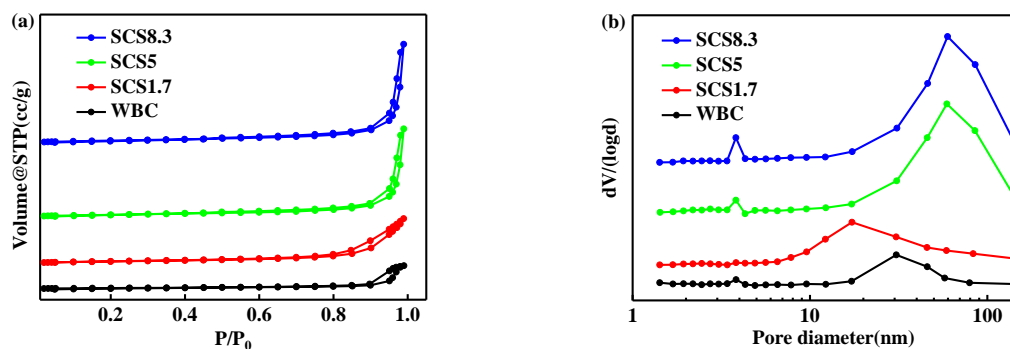
Table 2 showed the crystal size in the reduced catalysts calculated by Scherer formula. Clearly, the crystal size of SCS5 catalyst is smallest in all catalysts. In addition, to elaborate the relationship between reaction rate and crystal face growth of catalysts, the ratio of crystal sizes of D₂₁₁ and D₁₁₀ which represents the crystal face have the highest and minimum activity, respectively, and is listed in Table 2. The ratio of D₂₁₁/ D₁₁₀ in WBC catalyst is the biggest, and this means the best growth of (211) crystal faces. The ratio of crystal sizes is proportional to the activity of the catalyst.

2.2. Textural and Microstructural Properties of Catalysts

N₂ physical adsorption experiments were carried out to illustrate the specific surface area, and porosity of reduced catalysts. Table 3 shows the specific surface area, pore volume, and pore size of catalysts which were prepared by SCS with the different composition of glycine/Fe as well as WBC catalyst prepared by a traditional melting method. Clearly, the specific surface areas of the catalysts prepared by SCS reach 21.9 m² g⁻¹, which is significantly higher than that of WBC. After the high temperature melting, the WBC catalyst goes into a rapid cooling process and forms a dense solid, which leads to low surface area of the WBC catalyst. As indicated in Figure 2a, all catalysts show a type IV adsorption–desorption isotherm with an evident H3-Type hysteresis loop which suggests an irregular pore structure, implying that the catalysts are slit structure materials [13,14]. The distribution of pore size is plotted in Figure 2b. The most probable pore size is shown in Table 3.

Table 3. The N₂ physical adsorption results of the catalysts prepared by SCS and WBC catalyst.

Catalysts (Reduced)	S _{BET} (m ² ·g ⁻¹)	V _{pore} (ccg ⁻¹)	PD (nm)
WBC	4.9	0.05	30.7
SCS1.7	16.2	0.10	17.3
SCS5	16.4	0.02	59.2
SCS8.3	21.9	0.02	59.7

**Figure 2.** N₂ physical adsorption results for (SCS) and WBC catalyst. (a) The isotherms of N₂ adsorption-desorption and (b) BJH pore size distribution curves.

The morphology of fresh catalysts was characterized by the scanning electron microscopy technique (SEM) and the results are displayed in Figure 3. The fresh WBC catalysts are in the form of a large, grained, and dense solid. By contrast, SCS catalysts exhibit granular structure. Following the increase in glycine/Fe, the particle size decreases for SCS catalysts. With the ratio of SCS1.7 (glycine/Fe of 1.7), it formed relatively large particles and the particle size is between 500 nm and 1000 nm. This result is ascribed to the insufficient fuel [15]. According to the chemical equation, the stoichiometric ratio of the SCS1.7 is C₂H₅NO₂/Fe(NO₃)₃·9H₂O of 1.8. SCS5 and SCS8.3 catalysts possess the particle sizes of 100 nm to 500 nm [16]. It should be noted that a large amount of gas was produced during the SCS in a very short time [16–18]. The coarse surface and fine particles prepared by SCS are attributed to the flushing of gases during SCS.

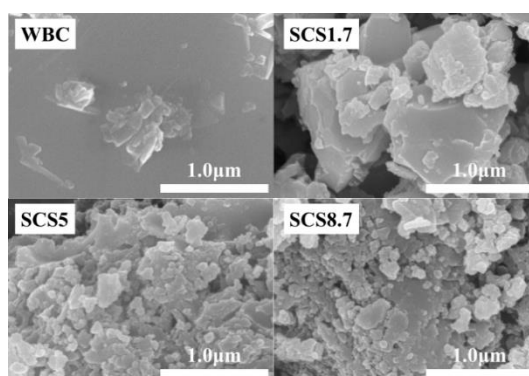
**Figure 3.** SEM images of the fresh glycine/Fe (SCS) and WBC catalyst.

Figure 4 illustrated the scanning electron microscope (SEM) images of the reduced SCS catalysts and WBC catalyst, as well as the surface element distribution mapping of Fe, Al, K, Ca, and overlapping images [19]. Evidently, significant surface segregation over the WBC catalyst was detected after reduction [20]. For WBC, most of the promoters, Al, K, and Ca, are distributed on the boundaries of Fe particles. By contrast, all the elements were uniformly dispersed over the SCS5 catalyst.

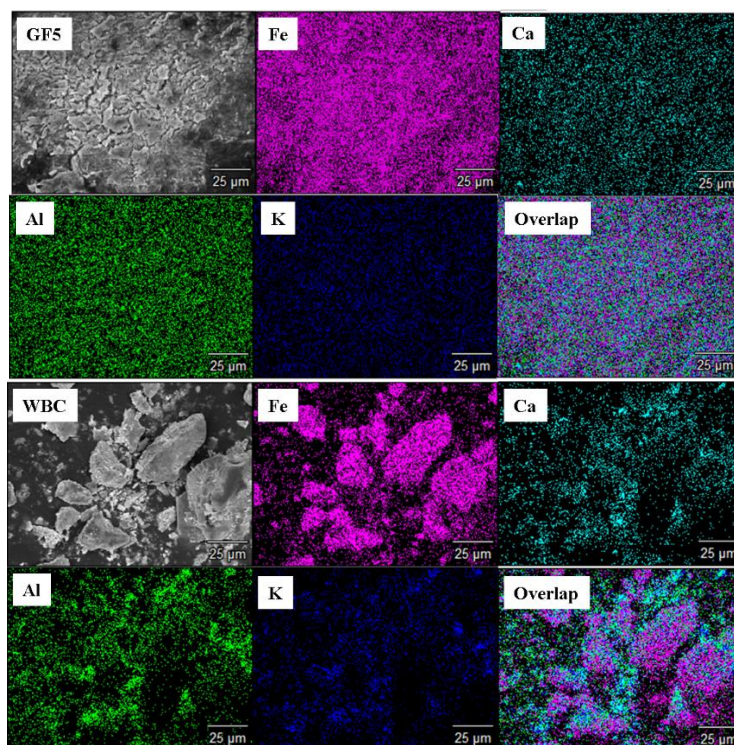


Figure 4. SEM images and EDS elemental mapping of SCS and WBC catalyst.

2.3. TEM Results

The reduced SCS5 and WBC catalysts were characterized by the TEM technique. The results were disclosed in Figure 5.

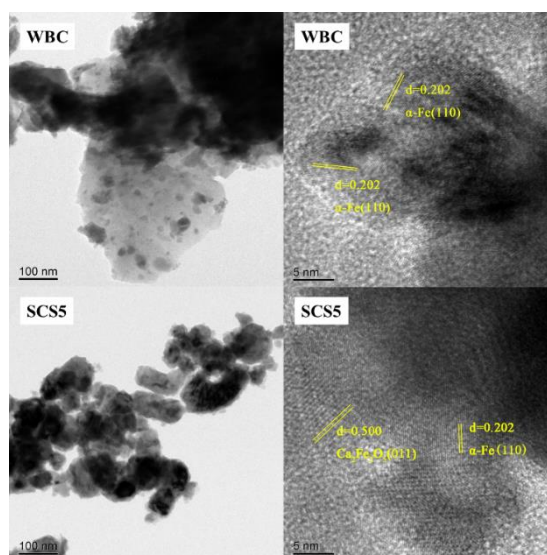


Figure 5. HR-TEM images of reduced SCS5 and WBC catalysts.

Obviously, the particle size of SCS5 catalyst is smaller than WBC catalyst, which is consistent with the results of SEM. The SCS5 catalyst has smaller particles than that of WBC [21–23]. A large number of bubbles were formed during SCS in very short time. When these bubbles eventually burst, it formed a stable solid catalyst. Clear fringe spaces of 0.202 nm corresponding to the (110) face of α -Fe were observed that is consistent with the XRD results in WBC and SCS5. We also observed clear fringe

spaces of 0.5 nm corresponding to the (011) face of $\text{Ca}_2\text{Fe}_2\text{O}_5$ indicating the formation of solid solution in the catalysts. The calcium oxide inhibits the disproportionation reaction of wüstite improving the catalytic activity. There are similar reports on this conclusion [24].

2.4. XPS Results

The XPS technique was adopted to identify the surface chemistry of the reduced catalysts. The whole XPS spectra indicate that the surfaces of both WBC and SCS5 catalysts are composed by Fe, O, K, Ca, and Al, according to Figure 6a, which is consistent with the result of SEM images and elemental mapping of EDS. In Figure 6b, the Fe 2p core levels split into 2p $3/2$ and 2p $1/2$ components because of the spin-orbit coupling. According to the literature, two peaks at binding energy 706.5 eV and 719.7 eV are related to the binding energies of Fe 2p $3/2$ and Fe 2p $1/2$ for Fe respectively [25–27]. The peaks which are located at 710.2 eV and 723.4 eV are attributed to Fe_2O_3 . Clearly, it suggests that the reduced catalyst was oxidized by air during the experiment. The peaks which are located at 714.5 eV and 727.7 eV are assigned to a solid solution of Fe [28–30].

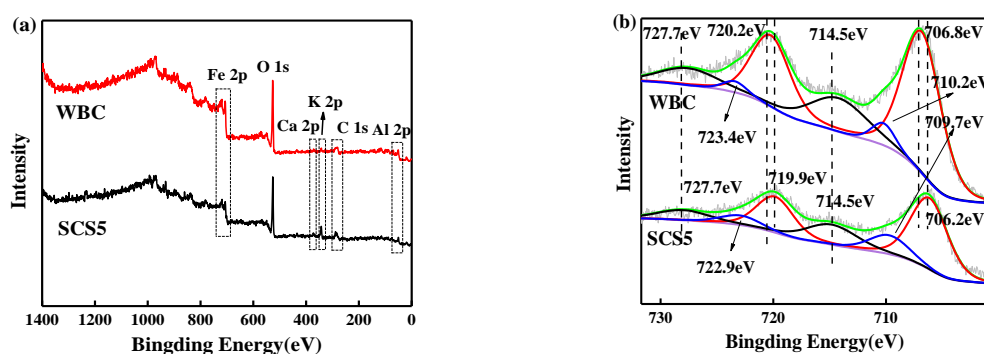


Figure 6. XPS spectra of reduced SCS5 and WBC catalyst; (a) the analysis of elements, (b) binding energy of Fe2p.

Compared with WBC, the binding energy of reduced Fe species shifts to a lower position significantly. It indicates that more electrons are transferred to the surface of Fe. The highest energy barrier in ammonia synthesis is the dissociative adsorption of N_2 molecules [31–33]. Consequently, it is the rate-limiting step for the iron-based catalyst. Electron rich Fe centers accelerate the dissociative adsorption of N_2 molecules, increasing the reaction rate of synthetic ammonia. According to Table 4, the peak area of Fe2p in WBC (13,025) is much larger than that of SCS5 (6328), which indicates the content of α -Fe in WBC is two times higher than that of SCS5. The ratios of Fe_s (solid solution of Fe) to simple Fe catalyst is 0.39 in SCS5 and this higher than that of WBC (0.35), which indicates more Fe to be buried in solid solution for SCS5 catalysts.

Table 4. The peak area of Fe, Fe in Solid solution and Fe_2O_3 species by XPS.

Catalysts	Fe2p ^a		Fe _s /Fe ^b
	Fe	Fe _s	
WBC	13,025 (706.8 eV, 720.2 eV)	4537 (714.5 eV, 727.7 eV)	0.35
SCS5	6328 (706.2 eV, 719.9 eV)	2445 (714.5 eV, 727.7 eV)	0.39

^a: represent the peak area of Fe and Fe_s from XPS peak fitting. ^b: the peak area ratio of Fe_s and Fe.

2.5. Catalytic Activity of Catalysts for Ammonia Synthesis

The catalytic activity for ammonia synthesis over SCS was evaluated and compared with WSC catalyst under the same conditions. Figure 7 and Table 5 give the ammonia concentration in the outlet of the reactor and its reaction rate at 15 MPa, 30,000 h⁻¹ and range of 400–450 °C. For all the catalysts

prepared by SCS, the ammonia synthesis reaction rate increases with fuel quantity before it reaches a sort of plateau until the glycine/Fe is 5. According to the XRD, the phase is α -Fe₂O₃ when the fuel is sufficient and is γ -Fe₂O₃ when the fuel is not sufficient. The α -Fe₂O₃ shows the better growth of (111) crystal planes compared with γ -Fe₂O₃. The more the crystal planes are exposed, the more active sites there are, and the higher the catalytic activity is. So, the catalytic activity of α -Fe₂O₃ is higher than that of γ -Fe₂O₃.

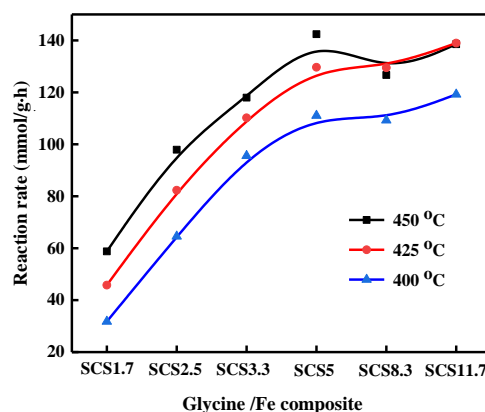


Figure 7. Reaction rate of ammonia synthesis over SCS catalysts with different glycine/Fe.

Table 5. Activity of catalyst prepared by solution combustion.

Samples	Weight /g	Activity of Catalyst for Ammonia Synthesis (15 MP, 30,000 h ⁻¹)					
		450 °C		425 °C		400 °C	
		vol.%	mmol/g·h	vol.%	mmol/g·h	vol.%	mmol/g·h
SCS1.7	2.27	12.26	130.30	11.24	116.93	9.22	97.69
SCS5	2.11	12.36	126.66	11.22	129.49	9.17	109.26
SCS8.3	1.94	12.36	138.52	11.48	138.95	9.44	119.21
WBC	6.06	18.60	69.32	18.82	70.01	17.35	65.35

It can be seen from Table 5 that the ammonia concentration is 12.36 vol.% for SCS5 with glycine/Fe of 5 and 18.60 vol.% for WBC at 450 °C, 15 MPa and 30,000 h⁻¹, respectively. Correspondingly, the reaction rate is 138.52 mmol g⁻¹ h⁻¹ for SCS5 and 69.32 mmol g⁻¹ h⁻¹ for WBC, respectively. Of note, although the ammonia concentration of SCS5 is lower than that of WBC, but the reaction rate is higher than that of WBC. This is because the reaction rate is proportional to the ammonia concentration and inversely proportional to the bulk density, while the bulk density of WBC is above three times higher than that of the SCS5 catalyst. Therefore, the catalytic activity of Fe₂O₃-based ammonia synthesis catalysts prepared by SCS still remains subject to a further increase.

3. Materials and Methods

3.1. Catalysts Preparation

Fe₂O₃-based ammonia synthesis catalysts with different fuel/Fe molar ratios were prepared by SCS. Fe(NO₃)₃·9H₂O (43.40 g, 99.0%, Aladdin, Shanghai, China), Al(NO₃)₃·9H₂O (2.22 g, 99.0%, Aladdin), KNO₃ (0.14 g, 99.0%, Aladdin, Shanghai, China), Ca(NO₃)₂·4H₂O (0.64 g, 99.0%, Aladdin, Shanghai, China) and glycine (14.46 g, 21.70 g, 28.93 g, 43.40 g, 72.30 g, 101.22 g, 99.0%, Aladdin, Shanghai, China) were dissolved in 150 mL distilled water. The solution was condensed in the 500 mL beaker in a water bath at 80 °C under mechanical stirring. Gelatinized samples were achieved and transferred into an alumina crucible. SCS was carried out at 500 °C in a muffle furnace for 3 h to obtain red fluffy material. Finally, it was pressed into pellets under 20 MPa for 15 min and then crushed into 1.0–1.4 mm particles.

WBC catalyst is a wustite-based catalyst prepared by melting according to our previous study [34,35]. In order to facilitate the explanation, the catalyst is named according to the glycine/Fe molar ratios listed in Supplementary Table S1. A WBC conventional catalyst was also prepared with the same content of promoters according to a methodology previously optimized by the authors.

3.2. Catalysts Characterization

N₂ physical adsorption (BET) experiment was measured by an ASAP2010 adsorption instrument (Micromeritics Company, Atlanta, GA, USA). The catalysts were degassed at 200 °C for 10 h before the analysis.

The phase and grain size of the catalysts were determined by X-ray diffraction (XRD) over a Bruker D8 Advance diffractometer ($\lambda = 0.154056$ nm, Cu K α radiation, $2\theta = 10^\circ\sim 140^\circ$) (Bruker AXS Company, Karlsruhe, Germany).

The morphology was investigated by SEM (scanning electron microscope, JSM-7800FPRIME) (Hitachi, Tokyo, Japan) with the accelerating voltage of 29 kV. The samples were crushed into a fine powder and sprayed with Pt to get clear images before the characterization of SEM. The surface element analysis of samples uses QUANTAX X-ray energy spectrometer (Bruker AXS Company, Karlsruhe, Germany).

The morphology and crystal structure of the samples were determined by TEM (transmission electron microscopy) using JEM-ARM300F GRAND ARM (JEOL, Akishima, Japan). The samples were crushed into a fine powder and dispersed in ethanol by ultrasonic treatment for 30 min before the characterization of TEM. Images were taken at an operating voltage of 160 kV.

For X-ray photoelectron spectroscopy (XPS) experiments, a spectrometer from Thermo ESCALAB 250XI photoelectron spectroscopy (Thermo Fisher Scientific Company, Waltham, MA, USA) with a mono-chromatized microfocused Al X-ray source was employed. Setting the binding energy of carbon (C1s) at 284.6 eV, the charging of samples was corrected. Before the measurements, the powder sample, pressed into self-supporting disks, was loaded into a sub-chamber and then evacuated at 25 °C for 4 h.

3.3. Catalytic Activity Test

To evaluate the catalytic activity of ammonia synthesis, the catalyst was placed in a fixed bed reactor (Figure 8) at high temperature (400 °C, 425 °C, and 450 °C) and high pressure (15 MPa). The reactor is a four-tube fixed-bed integral reactor (inner diameter 14 mm, isothermal zone 40 mm). A total of 2 mL (1.0–1.4 mm) catalyst was installed in the isothermal zone of the fixed bed reactor, and the upper and lower parts of the reactor bed were fixed with quartz sand.

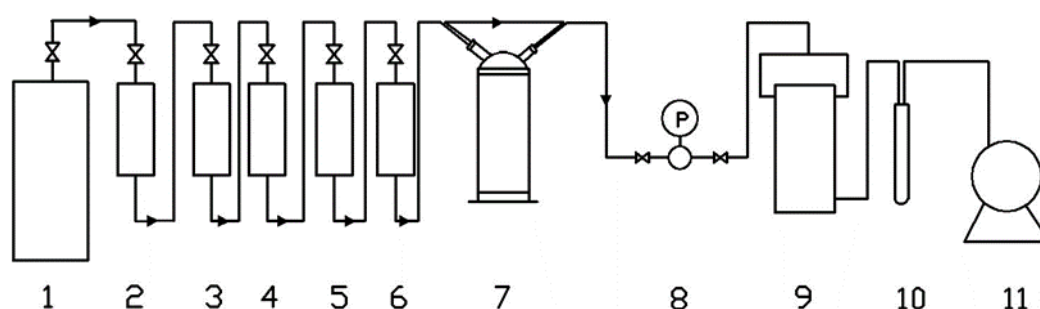


Figure 8. Process flow chart of ammonia synthesis catalyst performance evaluation unit. 1. liquid ammonia steel bottle; 2. ammonia cracking furnace; 3, 4, 5, 6. molecular sieve purification device; 7. compressor; 8. pressure regulating valve; 9. reactor; 10. gas absorption test tube; 11. wet flowmeter.

Hydrogen and nitrogen mixture with the molar composition of 3:1 was prepared by decomposition of liquid ammonia and purified by 5A molecular sieve, PdA molecular sieve, and 13X molecular sieve.

After purification, the hydrogen and nitrogen mixture was compressed by a diaphragm compressor to pass through a pipeline valve, and finally entered the reactor through the pressure stabilizing valve, controlling the flow rate of the gas in the reactor through the needle valve.

The catalyst was reduced by temperature programmed reduction (400 °C: 2 h, 425 °C: 6 h, 450 °C: 10 h, 475 °C: 4 h, 500 °C: 4 h) in mixed gas (75% H₂ and 25% N₂) according to the reduction procedure (5 MPa, 30,000 h⁻¹), then the reaction conditions (15 MPa, 30,000 h⁻¹) were controlled, and the formation rate of ammonia synthesis (Vol.%) was determined by sulfuric acid neutralization titration.

Ammonia concentration (φ) at the reactor outlet was calculated by Equation (1).

$$\varphi = \frac{N_{1/2\text{H}_2\text{SO}_4} \times V_{1/2\text{H}_2\text{SO}_4} \times 22.08}{N_{1/2\text{H}_2\text{SO}_4} \times V_{1/2\text{H}_2\text{SO}_4} \times 22.08 + V_2 \times K} = \left(1 + \frac{K \times V_2}{22.08 \times N_{1/2\text{H}_2\text{SO}_4} \times V_{1/2\text{H}_2\text{SO}_4}}\right)^{-1} \quad (1)$$

where $N_{1/2\text{H}_2\text{SO}_4}$ denotes the number of substance of 1/2 H₂SO₄, mol·ml⁻¹, $V_{1/2\text{H}_2\text{SO}_4}$ refers to the volume of sulfuric acid solution, in mL, 22.08 is the standard volume of ammonia gas, in L·mol⁻¹, V_2 is the residual gas volume measured by a wet-flow meter at the measurement conditions, in liters, and K is the conversion coefficient of the gas volume under the measurement conditions converting to gas volume at standard state.

$$K = \frac{P_0 - P_{\text{H}_2\text{O}}}{760(1 + t/273)} \quad (2)$$

where P_0 —atmospheric pressure, mmHg (1 mmHg = 133.322 Pa, the same below); $P_{\text{H}_2\text{O}}$ —saturated vapor partial pressure, mmHg; t —temperature of wet flow meter, °C. Reaction rate was determined by Equation (3).

$$r_m = \frac{S_V V_C}{22.41 W_C} \cdot \frac{\varphi - \varphi^0}{(1 + \varphi)} = \frac{S_V}{22.41 \rho_C} \cdot \frac{\Delta\varphi}{(1 + \varphi)} \quad (3)$$

where r_m —mass reaction rate, mmol·g⁻¹·h⁻¹; W_C —mass of reduced catalyst, g; V_C —volume of reduced catalyst, cm³; $\rho_C = \frac{W_C}{V_C}$ —packed density of reduced catalyst, g·cm⁻³; φ^0 , φ —ammonia concentration of the inlet and outlet of reactor, % (mol); $\Delta\varphi = \varphi - \varphi^0$ —net value of ammonia, %.

4. Conclusions

In this work, Fe₂O₃-based ammonia synthesis catalysts were prepared by SCS with Fe(NO₃)₃·9H₂O, Al(NO₃)₃·9H₂O, KNO₃, and Ca(NO₃)₂·4H₂O as the precursors and glycine as the fuel. The effect of different glycine/Fe ratios on catalyst performance was studied. The irregular granular catalysts were obtained in different theoretical fuel quantities. The α -Fe₂O₃ has a smaller particle size than the WBC catalyst, was obtained when the fuel was sufficient, and the promoters formed a more stable solid solution with Fe₂O₃.

The SCS5 catalysts prepared by SCS with high dispersion of promotions, shows higher ammonia synthesis reaction rate than that of traditional fused iron catalysts. The high dispersion of promoters, small iron particles in the catalyst, cause high activity and low energy consumption during the preparation of the catalyst. This is a useful attempt at the preparation of ammonia synthesis catalyst by the solution combustion method. Compared with the melting method, which requires high operating temperatures (1600 °C), SCS provides a simple and fast route for the preparation of catalysts for ammonia synthesis. Although the catalyst prepared by solution combustion synthesis presented a higher reaction rate than that of the catalyst prepared by a conventional melting method, it is in the form of powder and it is therefore difficult to press into pellets. In future work, the shaping of catalyst with proper mechanical strength will be focused upon. This work not only provides a new possibility for the industrial preparation of Fe-based catalysts for ammonia synthesis, but also provides a new direction for the development of Fe-based catalysts.

Supplementary Materials: The following are available online at <http://www.mdpi.com/2073-4344/10/9/1027/s1>, Table S1: Nomenclature of catalysts. Figure S1: Reaction rate of ammonia synthesis over citric acid/Fe composite catalysts prepared by SCS at a reaction condition. All the catalysts were reduced by temperature programmed reduction. Figure S2: Reaction rate of ammonia synthesis over glycol/Fe composite catalysts prepared by SCS at a reaction condition. All the catalysts were reduced by temperature programmed reduction. Figure S3: Reaction rate of ammonia synthesis over urea/Fe composite catalysts prepared by SCS at a reaction condition. All the catalysts were reduced by temperature programmed reduction.

Author Contributions: B.C.: Drafting the work; methodology and experimental investigation, literature search; figures; data collection. H.L.: acquisition; project supervision; funding acquisition. W.H.: Conceptualization, writing; project supervision; funding acquisition. All authors have read and agreed to the published version of the manuscript.

Funding: This research was funded by Zhejiang Provincial Natural Science Foundation of China under grant No. LY19B060009.

Conflicts of Interest: The authors declare no conflict of interest.

References

1. Liu, H.H. Recent advances in research of catalysts for ammonia synthesis. *Chin. J. Catal.* **2001**, *22*, 304–316.
2. Pernicone, N.; Ferrero, E.; Rossetti, I.; Forni, L.; Canton, P.; Riello, P.; Fagherazzi, G.; Signoretto, M.; Pinna, F. Wustite as a new precursor of industrial ammonia synthesis catalysts. *Appl. Catal. A Gen.* **2003**, *251*, 121–129. [[CrossRef](#)]
3. Liu, H.Z. Ammonia synthesis catalyst 100 years: Practice, enlightenment and challenge. *Chin. J. Catal.* **2014**, *35*, 1619–1640. [[CrossRef](#)]
4. Liu, H.Z.; Li, X.N.; Hu, Z.N. Development of novel low temperature and low pressure ammonia synthesis catalyst. *Appl. Catal. A Gen.* **1996**, *142*, 209–222. [[CrossRef](#)]
5. Han, W.F.; Huang, S.L.; Cheng, T.H.; Tang, H.D.; Li, Y.; Liu, H.Z. Promotion of Nb₂O₅ on the wustite-based iron catalyst for ammonia synthesis. *Appl. Surf. Sci.* **2015**, *353*, 17–23. [[CrossRef](#)]
6. Patil, K.C.; Aruna, S.T.; Mimani, T. Combustion synthesis: An update. *Curr. Opin. Solid State Mater. Sci.* **2002**, *6*, 507–512. [[CrossRef](#)]
7. Dinesha, M.L.; Jayanna, H.S.; Mohanty, S.; Ravi, S. Structural, electrical and magnetic properties of Co and Fe co-doped ZnO nanoparticles prepared by solution combustion method. *J. Alloys Compd.* **2010**, *490*, 618–623. [[CrossRef](#)]
8. Jin, Y.; Qin, W.P.; Zhang, J.S.; Zhang, M.M.; Wang, Y.; Cao, C.Y. Synthesis of Gd₃PO₇: Eu³⁺ nanospheres via a facile combustion method and optical properties. *J. Solid State Chem.* **2008**, *181*, 724–729. [[CrossRef](#)]
9. Lou, X.M.; Chen, D.H. Synthesis of CaWO₄: Eu³⁺ phosphor powders via a combustion process and its optical properties. *Mater. Lett.* **2008**, *62*, 1681–1684. [[CrossRef](#)]
10. Qiu, Z.F.; Zhou, Y.Y.; Lu, M.K.; Zhang, A.Y.; Ma, Q. Combustion synthesis of three-dimensional reticular-structured luminescence SrAl₂O₄: Eu, Dy nanocrystals. *Solid State Sci.* **2008**, *10*, 629–633. [[CrossRef](#)]
11. Wang, H.; Han, W.; Li, X.; Liu, B.; Tang, H.; Li, Y. Solution Combustion Synthesis of Cr₂O₃ Nanoparticles and the Catalytic Performance for Dehydrofluorination of 1,1,1,3,3-Pentafluoropropane to 1,3,3,3-Tetrafluoropropene. *Molecules* **2019**, *24*, 361. [[CrossRef](#)] [[PubMed](#)]
12. Zheng, Y.F.; Liu, H.Z.; Li, X.N. In situ X-ray Diffraction Investigation on Reduction Process of Ammonia-synthesis Fused-iron Catalysts and the Formation Mechanism of Its Active Phase. *Chem. J. Chin. Univ.* **2009**, *30*, 1177–1182.
13. Gu, B.; Ordonsky, V.V.; Bahri, M.; Ersen, O.; Chemayskii, P.A.; Filimonov, D.; Khodakov, A.Y. Effects of the promotion with bismuth and lead on direct synthesis of light olefins from syngas over carbon nanotube supported iron catalysts. *Appl. Catal. B Environ.* **2018**, *234*, 153–166. [[CrossRef](#)]
14. Li, J.B.; Ma, H.F.; Zhang, H.T.; Sun, Q.W.; Ying, W.Y.; Fang, D.Y. Direct production of light olefins from syngas over potassium modified Fe-Mn catalyst. *React. Kinet. Mech. Catal.* **2014**, *112*, 409–423. [[CrossRef](#)]
15. Ghosh, S.K.; Pal, S.; Roy, S.K.; Pal, S.K.; Basu, D. Modelling of flame temperature of solution combustion synthesis of nanocrystalline calcium hydroxyapatite material and its parametric optimization. *Bull. Mater. Sci.* **2010**, *33*, 339–350. [[CrossRef](#)]

16. Han, W.F.; Wang, Z.K.; Li, X.J.; Tang, H.D.; Xi, M.; Li, Y.; Liu, H.Z. Solution combustion synthesis of nano-chromia as catalyst for the dehydrofluorination of 1,1-difluoroethane. *J. Mater. Sci.* **2016**, *51*, 11002–11013. [[CrossRef](#)]
17. Gonzalez-Cortes, S.L.; Imbert, F.E. Fundamentals, properties and applications of solid catalysts prepared by solution combustion synthesis (SCS). *Appl. Catal. A Gen.* **2013**, *452*, 117–131. [[CrossRef](#)]
18. Han, W.F.; Liu, B.; Li, X.L.; Yang, L.T.; Wang, J.C.; Tang, H.D.; Liu, W.C. Combustion Synthesis of Amorphous Al and Cr Composite as the Catalyst for Dehydrofluorination of 1,1-Difluoroethane. *Ind. Eng. Chem. Res.* **2018**, *57*, 12774–12783. [[CrossRef](#)]
19. Tsuji, Y.; Kitano, M.; Kishida, K.; Sasase, M.; Yokoyama, T.; Hara, M.; Hosono, H. Ammonia synthesis over Co-Mo alloy nanoparticle catalyst prepared via sodium naphthalenide-driven reduction. *Chem. Commun.* **2016**, *52*, 14369–14372. [[CrossRef](#)]
20. Gupta, M.; Gupta, R.P. Anomalous surface segregation behaviour of some 3d elements in ferromagnetic iron. *J. Phys. Condens. Matter* **2013**, *25*, 8. [[CrossRef](#)]
21. Jafari, A.; Ebadi, A.; Sahebdehfar, S. Effect of iron oxide precursor on the properties and ammonia synthesis activity of fused iron catalysts. *React. Kinet. Mech. Catal.* **2019**, *126*, 307–325. [[CrossRef](#)]
22. Lendzion-Bielun, Z.; Jedrzejewski, R. Determination of the content of promoters in magnetite and wustite phases in the fused iron catalyst. *Pol. J. Chem. Technol.* **2013**, *15*, 27–29. [[CrossRef](#)]
23. Jedrzejewski, R.; Lendzion-Bielun, Z. Reduction Process of Iron Catalyst Precursors for Ammonia Synthesis Doped with Lithium Oxide. *Catalysts* **2018**, *8*, 494. [[CrossRef](#)]
24. Pu, Z.Y.; Zheng, Y.F.; Liu, H.Z.; Li, X.N. Influence of promoter and $\text{Fe}^{2+}/\text{Fe}^{3+}$ ratio on microstructure of fused iron catalysts for ammonia synthesis. *Indian J. Chem. Sect. A Inorg. Bio-Inorg. Phys. Theor. Anal. Chem.* **2011**, *50*, 156–162.
25. Powell, C.J. Recommended Auger parameters for 42 elemental solids. *J. Electron. Spectrosc. Relat. Phenom.* **2012**, *185*, 1–3. [[CrossRef](#)]
26. Ouyang, M.; Hiraoka, H. Structure and magnetic properties of iron oxide films deposited by excimer laser ablation of a metal-containing polymer. *Mater. Res. Bull.* **1997**, *32*, 1099–1107. [[CrossRef](#)]
27. Wu, H.B.; Desai, S.R.; Wang, L.S. Observation and photoelectron spectroscopic study of novel mono- and diiron oxide molecules: FeO_y^- ($y = 1-4$) and Fe_2O_y^- ($y = 1-5$). *J. Am. Chem. Soc.* **1996**, *118*, 5296–5301. [[CrossRef](#)]
28. Hara, M.; Kitano, M.; Hosono, H. Ru-Loaded $\text{C}_{12}\text{A}_7:e(-)$ Electride as a Catalyst for Ammonia Synthesis. *ACS Catal.* **2017**, *7*, 2313–2324. [[CrossRef](#)]
29. Kozuch, S.; Shaik, S. Kinetic-quantum chemical model for catalytic cycles: The Haber-Bosch process and the effect of reagent concentration. *J. Phys. Chem. A* **2008**, *112*, 6032–6041. [[CrossRef](#)]
30. Spencer, M.S. On the rate-determining step and the role of potassium in the catalytic synthesis of ammonia. *Catal. Lett.* **1992**, *13*, 45–54. [[CrossRef](#)]
31. Inoue, Y.; Kitano, M.; Kishida, K.; Abe, H.; Niwa, Y.; Sasase, M.; Fujita, Y.; Ishikawa, H.; Yokoyama, T.; Hara, M.; et al. Efficient and Stable Ammonia Synthesis by Self-Organized Flat Ru Nanoparticles on Calcium Amide. *ACS Catal.* **2016**, *6*, 7577–7584. [[CrossRef](#)]
32. Kitano, M.; Inoue, Y.; Yamazaki, Y.; Hayashi, F.; Kanbara, S.; Matsuishi, S.; Yokoyama, T.; Kim, S.W.; Hara, M.; Hosono, H. Ammonia synthesis using a stable electride as an electron donor and reversible hydrogen store. *Nat. Chem.* **2012**, *4*, 934–940. [[CrossRef](#)] [[PubMed](#)]
33. Kitano, M.; Kanbara, S.; Inoue, Y.; Kuganathan, N.; Sushko, P.V.; Yokoyama, T.; Hara, M.; Hosono, H. Electride support boosts nitrogen dissociation over ruthenium catalyst and shifts the bottleneck in ammonia synthesis. *Nat. Commun.* **2015**, *6*, 9. [[CrossRef](#)] [[PubMed](#)]
34. Liu, H.Z.; Liu, C.B.; Li, X.N.; Cen, Y.Q. Effect of an iron oxide precursor on the H_2 desorption performance for an ammonia synthesis catalyst. *Ind. Eng. Chem. Res.* **2003**, *42*, 1347–1349. [[CrossRef](#)]
35. Zheng, Y.-F.; Liu, H.-Z.; Liu, Z.-J.; Li, X.-N. In situ X-ray diffraction study of reduction processes of Fe_3O_4^- and Fe_{1-x}O -based ammonia-synthesis catalysts. *J. Solid State Chem.* **2009**, *182*, 2385–2391. [[CrossRef](#)]

